Effect of C and N and their absence on the kinetics of austenite-ferrite phase transformations in Fe-0.5Mn alloy

Farahani, Hussein; Zurob, Hatem; Hutchinson, Christopher R.; van der Zwaag, Sybrand

DOI
10.1016/j.actamat.2018.03.026

Publication date
2018

Document Version
Final published version

Published in
Acta Materialia

Acta Materialia 150 (2018) 224–235

Contents lists available at ScienceDirect

Acta Materialia

journal homepage: www.elsevier.com/locate/actamat

Effect of C and N and their absence on the kinetics of austenite-ferrite phase transformations in Fe-0.5Mn alloy

Hussein Farahani [a, *], Hatem Zurob [b], Christopher R. Hutchinson [c], Sybrand van der Zwaag [a]

[a] Faculty of Aerospace Engineering, Delft University of Technology, Delft, The Netherlands
[b] Department of Materials Science and Engineering, McMaster University, Hamilton, ON, Canada
[c] Department of Materials Science and Engineering, Monash University, Clayton, 3800, Vic, Australia

ARTICLE INFO

Article history:
Received 15 November 2017
Received in revised form
6 March 2018
Accepted 13 March 2018
Available online 16 March 2018

ABSTRACT

Investigating the partitioning effect of substitutional and interstitial elements on the migration of transformation interfaces during austenite-ferrite phase transformation in steels with the conventional experimental method is extremely challenging due to interaction between the solute atoms and the transformation interfaces. Additionally, the simultaneous nucleation of new phases during phase transformations limits the accuracy of extracted growth rates from experimental kinetics measurements of phase fractions. In a novel experimental approach, the cyclic partial phase transformation concept is used to avoid the effect of nucleation on total kinetics of phase transformations. In this study, a Fe-0.5Mn alloy in the presence and absence of interstitial C and N additions is subjected to different cyclic transformation routes to examine the possible interaction between solute atoms and migrating interfaces. The experimental results are in semi-quantitative agreement with modelling predictions made by the local equilibrium approach and provide indirect evidence of Mn partitioning at austenite/ferrite interface in absence of any interstitial elements. It is also confirmed that the presence of interstitial elements promotes Mn interaction with the interface, whereas N promotes more Mn partitioning at transformation interface compared to C.

1. Introduction

The precipitation of ferrite during austenite decomposition is a key step in the microstructure evolution of many important steel grades. The transformation kinetics in Fe-X-Y systems is complicated by the large difference in the diffusion rates of the interstitial elements, Y= C, N and the substitutional elements, X = Mn, Ni, Si, Mo … etc., along with the possible interactions of the elements with the transformation interfaces [1].

In a given industrial condition, ferrite formation may occur with or without partitioning of the substitutional alloying element between phases [2–5]. This leads to complex situations in which the kinetics of phase transformation in a Fe-X-Y steels can be controlled by the short-range or long-range or interfacial diffusion of substitutional and interstitial elements. This is not say, however, that these effects can be simply assumed separated. In many conditions, the interaction of substitutional element with the transformation interfaces strongly influences [6,7] or is influenced [8] by concentration of interstitial elements at the interface.

Several experimental and theoretical attempts have been conducted to capture effect of substitutional (especially Mn) and interstitial solutes (especially C and N) on the interface migration during austenite to ferrite phase transformation. In a simple approach, the individual effect of solutes on the austenite to ferrite phase transformation can be studied separately in binary Fe-C, Fe-N and Fe-Mn systems. On top of theoretical differences between effects of C and N in Fe-based alloys predicted by atomistic simulations [9,10], it has been experimentally shown that [11–13] in Fe-N system with low nitrogen, austenite to ferrite transformation occurs massively and the interface velocity is independent of the cooling rate, while in Fe-C system the transition from interface controlled to diffusion controlled regimes delimits transformation kinetics. In the Fe-Mn system, the austenite to ferrite transformation occurs massively with a large change in strain energy caused by misfit between the two phases. All these data provide

* Corresponding author.
E-mail address: h.farahani@tudelft.nl (H. Farahani).

https://doi.org/10.1016/j.actamat.2018.03.026
1359-6454/

useful basics to explain characteristic effects of each individual element on a migrating austenite/ferrite interface. However, a simple combination of these findings fails in making accurate predictions for ternary Fe-X-Mn systems, suggesting a potential role of interatomic interactions between solutes at interfaces.

In another approach, the effects can be studied by conducting austenite to ferrite phase transformation experiments in series of Fe-C-Mn and Fe-N-Mn ternary steels. In this regard, a series of recent experimental studies on ferrite growth during controlled decarburizing and denitriding [14,15], have suggested interfacial segregation of Mn in presence of C, but no sign of interfacial segregation of Mn in Fe-N-Mn. These findings, based on analysis of the growth kinetic data, is consistent with the preceding accepted perception [8,16–18] that the presence of interstitial elements influences the tendency of the substitutional alloying element to segregate to the interface. However, the very slow and continuous ferrite growth in decarburizing and denitriding condition is quite different from the conventional ferrite precipitation reaction in which ferrite passes from fast transformation to a stasis regime [19,20], makes generalization of these findings difficult.

In parallel to experiment, theoretical works also confirm the importance of the interaction of solute elements at the interfaces. Recent ab-inito calculations by Wicaksono et al. [21] confirm strong attractive interaction between C and Mn in bulk bcc iron at the atomistic scale. This is in agreement with the study on ferrite transformation stasis by Sun et al. [22] using a coupled solute drag model, stating that repulsive or attractive interaction between interstitial and substitutional elements can directly influence the interfacial behaviour of substitutional elements. As an example, Si interaction with a migrating austenite/ferrite interface in a Fe-C-Y steel can be very different in the presence or absence of Mn [23].

Underlining the effect of solutes on migrating austenite/ferrite interfaces, one should remember that the experimentally measured kinetics of austenite to ferrite transformation is a product of both nucleation and growth. Addition of substitutional elements to Fe-C and Fe-N binary steels have a strong effect on the nucleation kinetics [24,25]. In recent years, development of the Cyclic Partial Phase Transformation (CPPT) concept, made it possible to study the effect of alloying elements on migration of the austenite/ferrite interface without the complications associated with concurrent nucleation [26–28]. In a CPPT experiment, the temperature is cycled inside the intercritical zone where both austenite and ferrite phases are present at all times. The CPPT concept has been successfully used to study, both experimentally and theoretically, the effect of substitutional elements, especially Mn, on the migration rate of austenite/ferrite interfaces. A stagnant stage, during which the growth of ferrite (or austenite) is significantly delayed, is found in Fe-C-Mn alloys, while no stagnant stage is observed in Fe-C alloys. While the reported increasing magnitude of the growth retardation with increasing concentration of substitutional elements (i.e. Mn or Ni) is attributed to strong partitioning behavior of substitutional elements at transformation interfaces [29], the role of interstitial elements on the partitioning behavior of substitutional elements is still unknown.

The approach of changing the bulk interstitial solute content in order to evaluate the effect of the X-Y interaction is not easily adapted to phase interfaces. Instead, in this study we have used CPPT concept to examine this possible interaction in an Fe-0.5Mn alloy in the presence and absence of interstitial C and N additions. The kinetics measurement in Fe-C-Mn, Fe-Mn and Fe-N-Mn systems will open windows to better understand the extent to which the presence of Mn at the interface is dictated by the Mn-interface interaction as opposed to the interaction of Mn with the interstitial elements present at the interface.

2. Decarburization and nitriding experiments

An Fe-0.1C-0.5Mn steel was selected as the starting alloy for this study. In order to prepare interstitial free alloys, hollow cylindrical samples with length of 10 mm, diameter of 5 mm and thickness of 1 mm were subject to controlled decarburization to produce the binary Fe-0.5Mn alloy. The ternary Fe-N-Mn alloys were then produced using controlled nitriding of the Fe-0.5Mn binary. The full details for these processes are given by Guo et al. [14]. The exact composition of the alloys used in this study are shown in Table 1. While we intended to make the nitrogen concentration equal to the original carbon concentration, we did not succeed, but as explained in the next section we could compensate for the difference in concentration level by adjusting the temperature ranges over which to cycle.

3. The cyclic heat treatments

All heat treatments were performed using a Bähr DIL 805A/D/T Quenching Dilatometer. Two thermocouples, spaced 4 mm apart, were attached to the specimen to measure the temperature difference in the sample precisely. All the specimens were heated with a rate of 10K/s to 1173K(900 °C) and kept for 300s(5 min) to ensure full austenitization. The samples were then subjected to different Cyclic Partial Phase Transformation (CPPT) routes and Continuous Cooling (CC) experiments with cooling (or heating) rates of 1K/s as shown in Fig. 1, with the exact treatment temperatures indicated in Table 1 for each alloy.

In a continuous cooling (CC) experiment (Fig. 1a), the sample is cooled at a constant rate of 1K/s from the austenitization temperature to a temperature below the A_1 transition temperature. During cooling, the kinetics of austenite to ferrite phase transformation is controlled via concurrent nucleation and growth events, in consort with continuous segregation of Mn at the newly formed austenite/ferrite interfaces and redistribution of interstitial element in the remaining austenite. In a type H CPPT experiment, as shown in Fig. 1b, the sample is continuously cooled to T_1, below A_3 and inside the intercritical region, kept isothermally for 20 min, leading to a mixture of austenite and ferrite with the formation of Mn spike at the interfaces and redistribution of interstitial elements (C or N) around the interface resulting in a minimal compositional gradient. Then, the temperature is increased to T_2, still inside the austenite/ferrite two phase region, and again kept isothermally for 20 min to give enough time for Mn interaction with the interface and redistribution of interstitial elements before final cooling to room temperature. In type I CPPT experiment (Fig. 1c), temperature is cycled between T_1 and T_2, but immediate changes in temperature after reaching T_1 and T_2 are used in order to limit the time available for the redistribution of interstitial elements. Type H-I and I-H (Fig. 1d and e) cyclic experiments are designed to generate a spike of Mn at the interface, with controlled redistribution of the interstitial element only at T_1 or T_2, through one isothermal holding stage at T_1 or T_2, and sudden changes in temperature after reaching T_2 or T_1, respectively.

One of the subtle aspects of the experimental work concerns the stability of the Fe-N-Mn solution against decomposition into ferrite and nitrogen gas. In order to avoid decomposition during the present experiments, it was necessary to work with dilute N contents. The Fe-N-Mn samples were also coated using gold sputtering to prevent possible nitrogen bubble formation during thermal experiments in the dilatometer [30]. The microstructure of all of the samples were checked before and after the experiments to confirm the reliability of the experimental results. In each case, the experiments were performed at least twice to ensure the reproducibility of the results. The microstructures after the experiments were

Table 1
Compositions of the alloys used in the experiments.

Alloy name	Exact Composition (all in wt.%)	T_1	T_2
Fe-0.1C-0.5Mn	Fe-0.0848C-0.47Mn	775 °C (1048K)	825 °C (1098K)
Fe-0.5Mn	Fe-0.01C-0.47Mn	860 °C (1133K)	885 °C (1158K)
Fe-0.3N-0.5Mn	Fe-0.27N-0.47Mn	685 °C (958K)	735 °C (1008K)

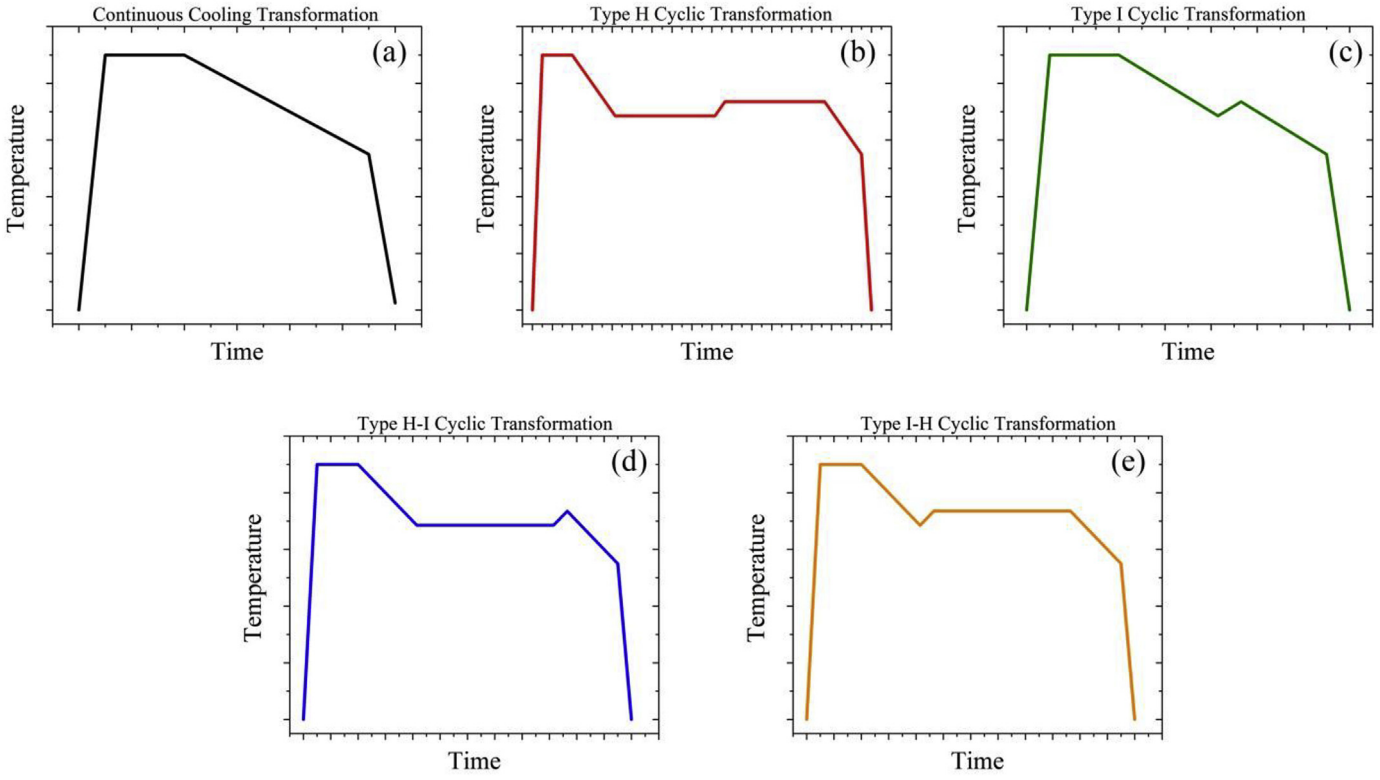

Fig. 1. Different applied experimental thermal routes.

checked to make sure the amount of possible decarburization or denitriding during experiments was negligible.

4. Modeling details

Simulations of cyclic phase transformations and continuous cooling experiments are performed in different composition sets of Fe-C-Mn, Fe-Mn and Fe-N-Mn systems. For all simulations a 1-D geometry with a size of $25\mu m$ is assumed to represent austenite grain size of $50\mu m$. Simulations are carried out using the DICTRA software linked to TCFE7 and MOB2 databases. For each composition, the Ae_1 and Ae_3 temperatures are calculated with Thermo-Calc software [31]. The cyclic transformation temperatures, T_1 and T_2, are selected as $T_1 = \frac{(Ae_3+Ae_1)}{2} - \Delta T/2$ and $T_2 = \frac{(Ae_3+Ae_1)}{2} + \Delta T/2$, where $\Delta T = 50K$ for Fe-C-Mn and Fe-N-Mn systems and $\Delta T = 25K$ for Fe-Mn system.

5. Results

In this section, the results of the dilatometry experiments and LE modeling for all three systems subjected to different thermal routes are presented. For better comparisons in all of the dilatation graphs, the Y axis displays the absolute difference between recorded dilatation at temperature T and total dilatation at austenitization temperature of 1173K(900 °C). Results of modeling are illustrated in graphs of 'superposed interface position' vs temperature and are plotted next to experimental results. In order to direct comparison of the modeling and experimental graphs, the interface position in modeling graphs are modified by applying the effect of thermal expansion/contraction with a constant coefficient of thermal expansion of 0.2 μm/K for both austenite and ferrite.

Fig. 2 shows the experimental and modeling results for CC and type H CPPT routes in Fe-0.1C-0.5Mn, Fe-0.5Mn and Fe-0.3N-0.5Mn alloys. The experimental CC curve in Fe-0.1C-0.5Mn alloy (Fig. 2a) indicates a steady austenite to ferrite phase transformation, while the dilatation curve for the type H CPPT route between $T_1 = 1048K(775\,°C)$ and $T_2 = 1098K(825\,°C)$ shows different distinct stages of phase transformation. In this route, austenite to ferrite phase transformation starts during cooling and continues during the isothermal holding stage (20 min) at $T_1 = 1048K(775\,°C)$. By heating from T_1 up to about 1073K(800 °C), the so-called 'stagnant stage' [27] starts, during which a linear thermal expansion is observed and no phase transformation or austenite/ferrite interface migration occurs. Upon further heating, the nonlinear contraction is the signature of the 'direct transformation stage' during which ferrite transforms partially to austenite. After isothermal ferrite to austenite transformation in the course of holding at $T_2 = 1098K(825\,°C)$ for 20 min, the linear contraction during cooling from 1098K(825 °C) to about 1073K(800 °C) indicates a stagnant stage in ferrite formation followed by direct austenite to

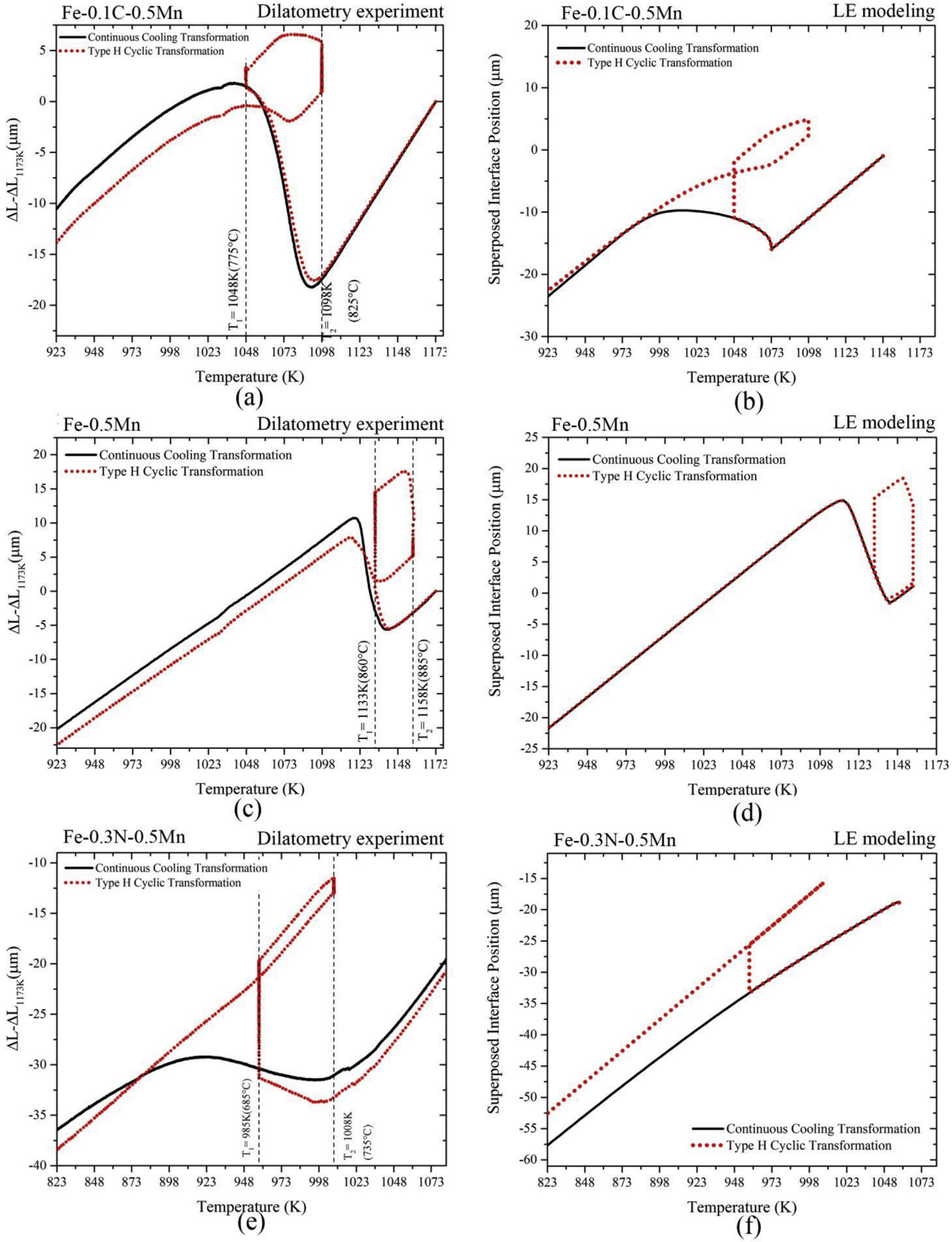

Fig. 2. Experimental dilation curves and modeling results for CC transformation vs type H CPPT in Fe-0.1C-0.5Mn, Fe-0.5Mn and Fe-0.3N-0.5Mn alloys.

ferrite transformation stage upon further cooling. The corresponding results of LE modeling in the Fe-0.1C-0.5Mn alloy are shown in Fig. 2b. Analogous to the experiments, the CC curve in Fig. 2b displays a smooth growth for ferrite with slightly different onset temperature compared to the experimental curve. The isothermal direct transformation stage, stagnant stage and non-isothermal transformation stage, which are observed during the type H CPPT experiment are all well captured by the LE model. The length of the stagnant stage, during which the austenite/ferrite interface in the model does not move in spite of temperature variation, is predicted to be 25K, in close agreement with the corresponding experimental observation.

The experimental dilatation and modeling of CC and type H CPPT curves for the binary Fe-0.5Mn alloy are shown in Fig. 2c and d, respectively. Similar to the carbon containing system, both the experimental and simulated CC curves show steady austenite to ferrite phase transformation during cooling. Regardless of the absence of interstitial elements in this alloy, the experimental type H CPPT curve displays stagnant stages in both austenite to ferrite and ferrite to austenite phase transformations after isothermal holdings at $T_1 = 1133K(860\,^{\circ}C)$ and $T_2 = 1158K(865\,^{\circ}C)$ with an approximate length of 20K, which is well-captured by the interface position model in Fig. 2d.

For the Fe-0.3N-0.5Mn alloy, the austenite to ferrite phase transformation during continuous cooling is similar to that observed in the other two alloys as shown in Fig. 2e. A number of differences are observed, however, in the type H cyclic curve between $T_1 = 958K(685\,^{\circ}C)$ and $T_2 = 1008K(735\,^{\circ}C)$ in the nitrided system compared to the other two systems. The length of stagnant stages in ferrite to austenite (during heating) and austenite to ferrite (during second cooling) transformations are substantially different. In type H CPPT curve, the austenite to ferrite transformation is inactive for heating up to about 45K. However, the linear contraction of the specimen for more than 180K during cooling cycle after the isothermal stage at T_2, indicates to a very long stagnant stage for ferrite formation in the second cooling cycle.

As with the experimental dilatation curves, the modeling results in Fe-0.3N-0.5Mn shown in Fig. 2f, are also quite different from the other two alloys. While the CC curve predicts a smooth ferrite growth during continuous cooling, in type H CPPT after the first isothermal holding at T_1, the interface remains immobile during heating and isothermal holding at T_2. The prediction of an immobile interface during heating and isothermal holding differs from the experimentally observed direct isothermal transformation stage at T_2. Upon final cooling down to $823K(550\,^{\circ}C)$, the LE model predicts no interface motion, consistent with the experimental observation in Fig. 2e.

The results of type I vs type H CPPT experiments and modeling for the three alloys are shown in Fig. 3. The dilatation curves for the Fe-0.1C-0.5Mn alloy in Fig. 3a show slightly different behavior of the alloy when subjected to type I cyclic treatments. In the type I curve, at the onset of heating from T_1 in the first cycle, the nonlinear expansion for about 10K points to continuation of austenite to ferrite transformation, notwithstanding heating of the sample; this part is referred as 'inverse transformation stage'. The subsequent linear expansion and nonlinear contraction by further heating to T_2, are signatures of the ferrite to austenite stagnant stage and the direct transformation stage, respectively. Unlike heating, no inverse transformation stage is observed after an immediate change in temperature, as the linear contraction during cooling indicates a stagnant stage followed by nonlinear expansion due to austenite to ferrite transformation upon further cooling. In the modeling results of type I (Fig. 3b), the interface migration into the austenite region in spite of the temperature increase points to the inverse transformation stage. This is followed by a stagnant stage, occurring during the cooling cycle with a similar length to type H.

In the type I experimental curve for Fe-0.5Mn alloy (Fig. 3c), the respective expansion and contraction curves for heating and cooling cycles between T_1 and T_2 appear linear, but not perfectly parallel. This indicates a very short and negligible inverse transformation stage at the onset of heating/cooling cycles. The corresponding modeling curve in Fig. 3d successfully captures the experimental stagnant stage as well as the very short inverse transformation stage which is distinguishable by backward interface migration in the modeling results.

For the Fe-0.3N-0.5Mn alloy, according to the observed nonlinear dilatation curves of the type I CPPT in Fig. 3e, the inverse transformation stage expands for the whole length of heating cycle. The short linear contraction of about 10K after immediate change in the temperature regime corresponds to the stagnant stage followed by a short nonlinear stage promoted by negligible austenite to ferrite transformation and linear contraction in the final cooling. In the simulated curve for type I CPPT (Fig. 3f), the interface sluggishly moves into the austenite region during heating and becomes immobile after that. This interface migration manner is comparable to the slow inverse transformation stages observed in the experiment.

The experimental and modeling curves for H-I and I-H CPPT routes are shown in Fig. 4. As expected for the Fe-0.1C-0.5Mn alloy (Fig. 4a), in type H-I during the first isothermal holding and heating cycle, the dilatation curve points to an isothermal transformation stage, a stagnant stage and a direct transformation stage similar to the type H curve. The cooling curve is similar to type I, and displays austenite to ferrite stagnant stage and direct transformation stages. In type I-H curve, a short nonlinear expansion due to the inverse austenite to ferrite transformation is also found at the onset of the heating stage, similar to type I, followed by stagnant stage. The dilatation behavior of the specimen during the rest of the thermal cycle is identical to the one subjected to type H cyclic experiment. The type H-I modeling curve (Fig. 4b), captures well the experimentally observed stages during heating. However, in the cooling cycle after the stagnant stage, there is an abrupt change in interface velocity during its migration into the austenite region, which could be caused by interaction with the residual Mn spike formed at the end of the isothermal heating stage at T_1. The smooth interface migration in type I-H curve, demonstrates the inverse transformation, stagnant stage and direct transformation stages.

Analogous to the Fe-0.1C-0.5Mn alloy, the dilatation curves for type H-I and I-H CPPT experiments in the Fe-0.5Mn alloy (Fig. 4c), exhibit mixed behavior in heating/cooling corresponding to type H and type I, with an stagnant stage of 20K and negligible inverse transformation stage. The modeling results for Fe-0.5Mn alloy (Fig. 4d) nicely capture the experimentally observed transformation features in dilatation curves; similar to type I c, the very short inverse transformation stages in type I-H CPPT curves is discernible by backward interface migration in the modeling results.

In Fe-0.3N-0.5Mn alloy (Fig. 4e), the dilatation curve for the type H-I CPPT route, is analogues to the type H curve, but without a direct isothermal transformation stage at T_2. During holding at T_2 in type I-H experiment, a new stage of 'isothermal inverse transformation' is observed corresponding to the continued austenite to ferrite phase transformation, notwithstanding the 50K rise in the temperature and 20 min of isothermal holding. The LE model results for type H-I and I-H CPPT routes (Fig. 4f), are very similar to

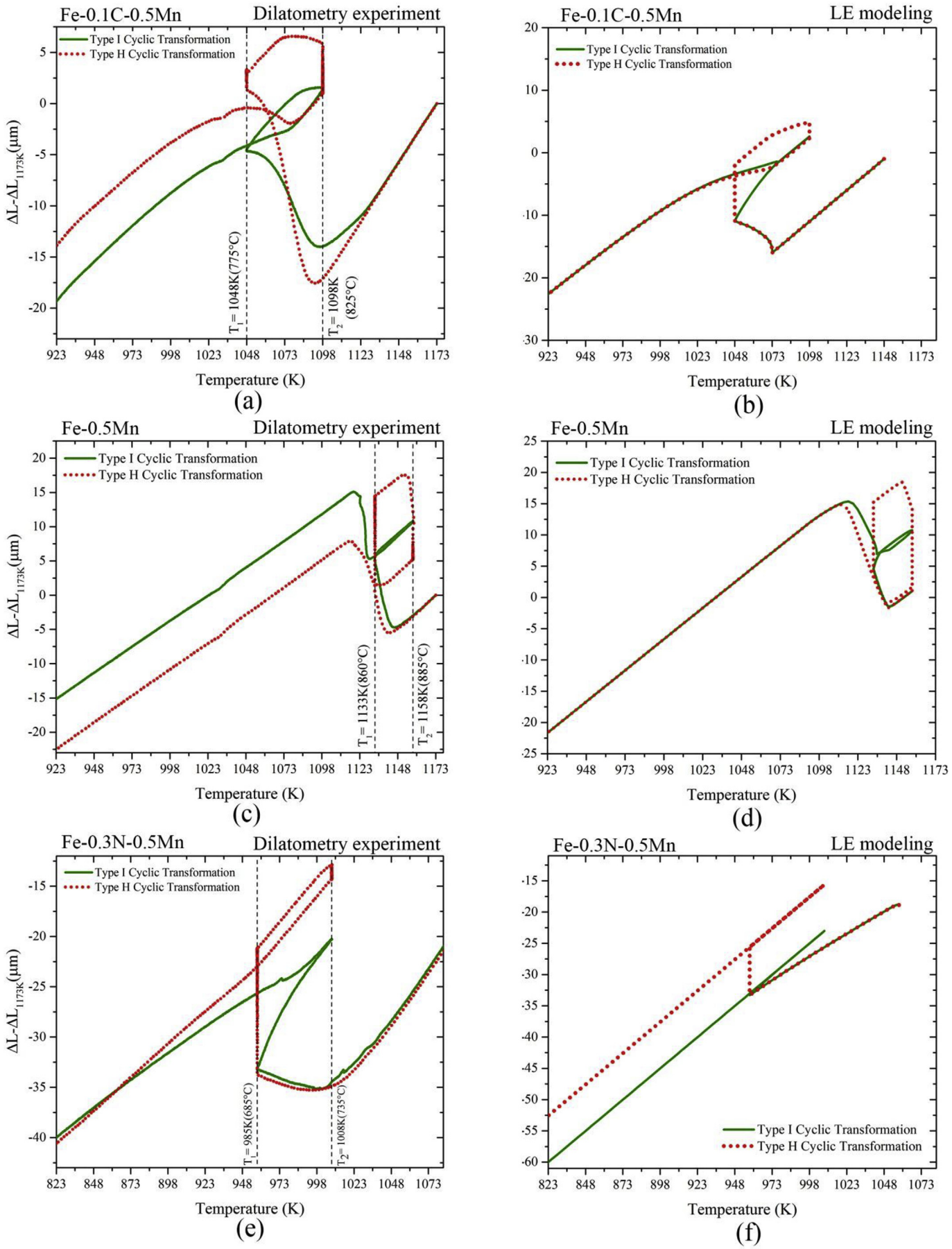

Fig. 3. Experimental dilation curves and modeling results for type I vs type H CPPT in Fe-0.1C-0.5Mn, Fe-0.5Mn and Fe-0.3N-0.5Mn alloys.

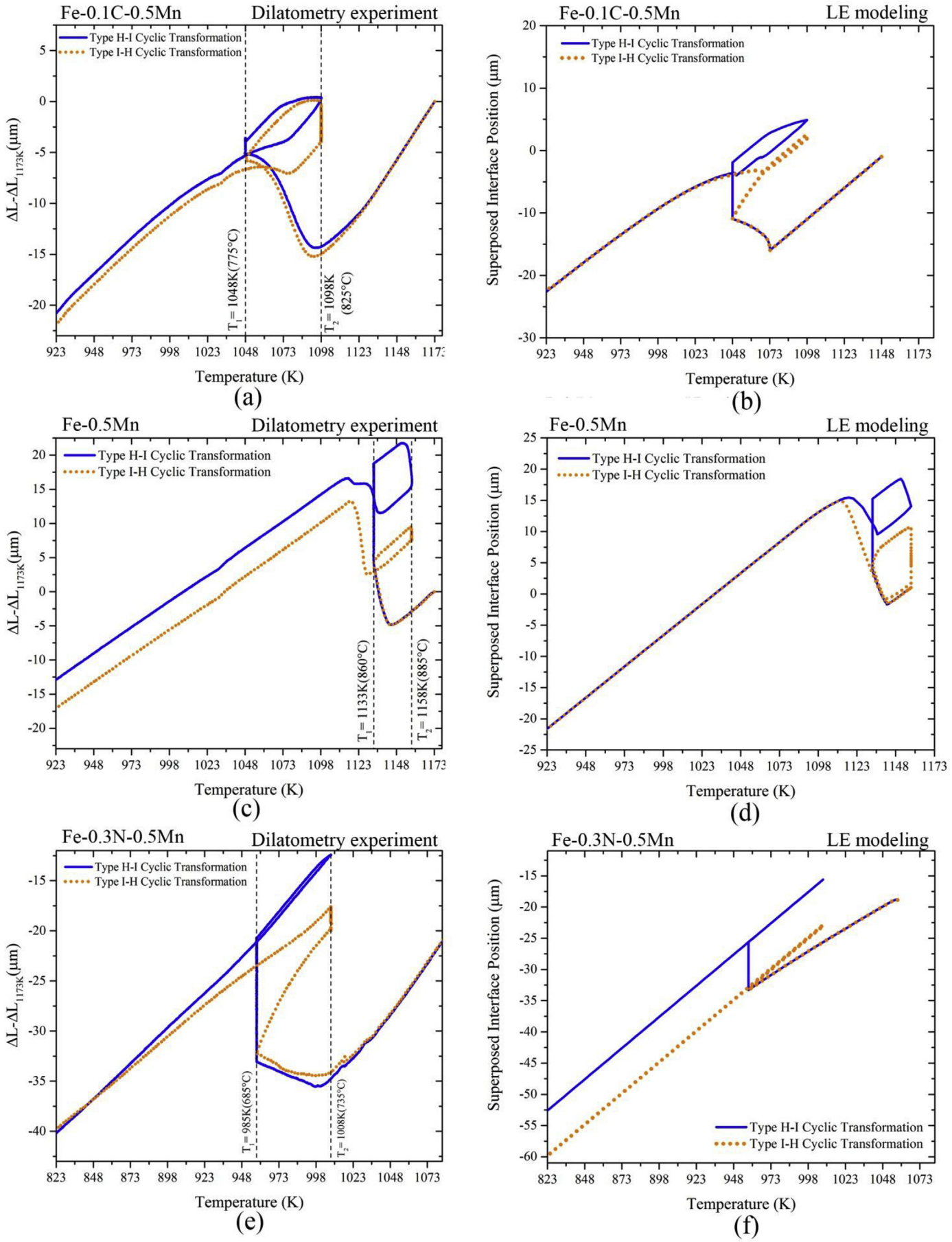

Fig. 4. Experimental dilation curves and modeling results for type H-I vs type I-H CPPT in Fe-0.1C-0.5Mn, Fe-0.5Mn and Fe-0.3N-0.5Mn alloys.

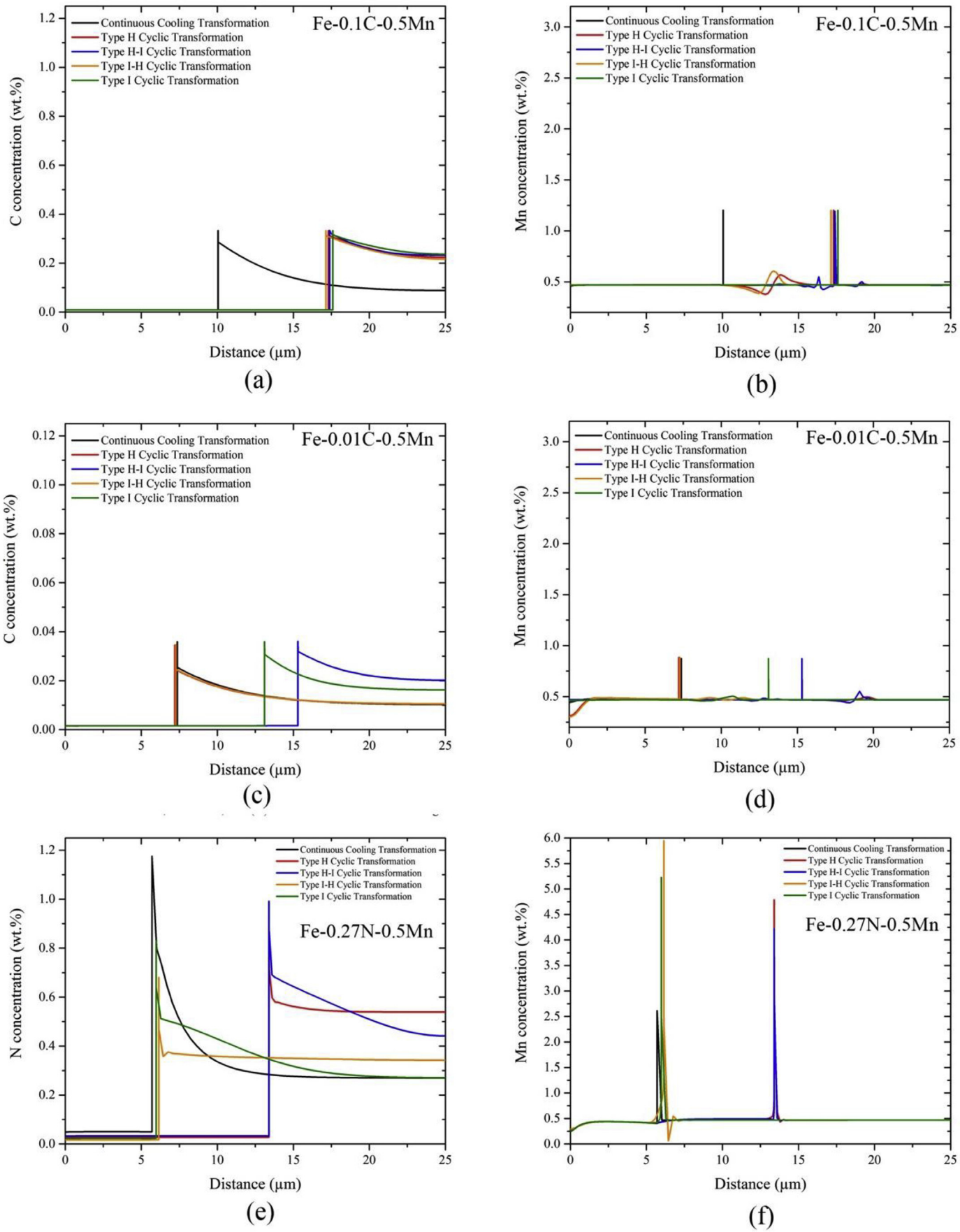

Fig. 5. Profiles of Mn and C/N before the final cooling at T_1 in LE modeling of different thermal routes.

the predictions for type H and type I routes. In addition, no isothermal inverse transformation stage at T_2 is predicted in the type I-H route.

In summary, the dilatation curves for the Fe-0.1C-0.5Mn alloy show four different transformation stages. The length of the stagnant stage in both austenite and ferrite formation is about 25K. The inverse transformation stage is observed for about 10K. The stagnant stage, with a length of 20K, is still observed in the decarburized Fe-0.5Mn alloy. The dilatation behavior in the Fe-0.3N-0.5Mn alloy is quite different, with longer stagnant stages both in heating and cooling cycles, as well as protracted inverse transformation stages.

6. Discussion

The differences in the observed behavior between the different CPPT routes and continuous cooling experiments in the three Fe-0.1C-0.5Mn, Fe-0.5Mn and Fe-0.3N-0.5Mn systems are semi-quantitatively captured by LE model. Thus, it is expected that the features observed by experiments can be explained by analyzing the results of the LE model.

The profile of Mn and interstitial elements (C or N) after cyclic experiments at T_1 before the final cooling for all of the thermal routes are shown in Fig. 5 a–f. It can be seen that the profiles in type H show a spike of Mn at the interface, zig-zag partitioning of Mn at the former position of the interface after the second isothermal

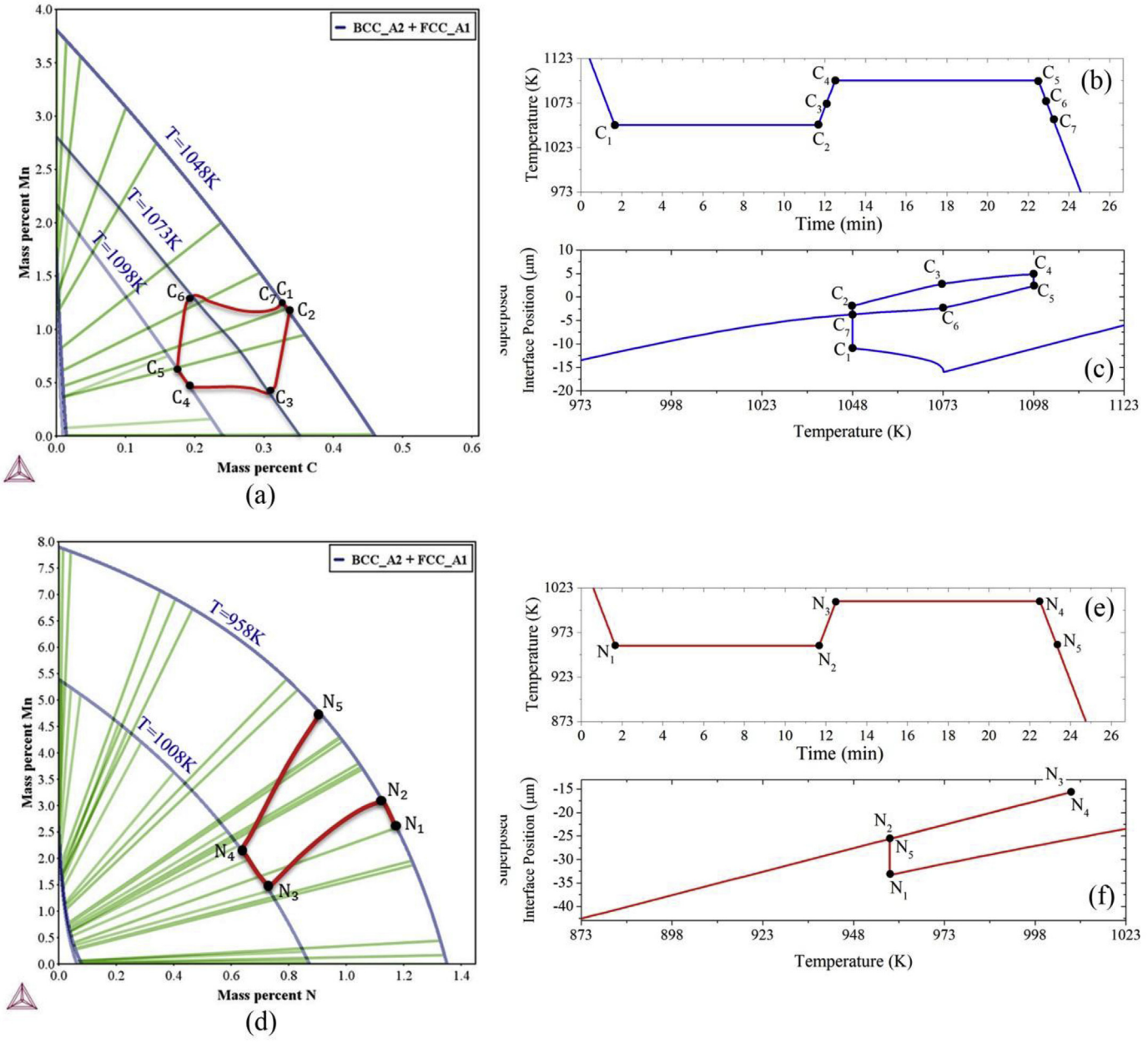

Fig. 6. a) Isothermal section of Fe-C-Mn phase diagram, b)applied thermal route, c) LE model results of type H CPPT in Fe-0.1C-0.5Mn alloy, d) Isothermal section of Fe-N-Mn phase diagram, e)applied thermal route, f) LE model results of type H CPPT in Fe-0.3N-0.5Mn alloy.

holding at T_2, a broadened bulge of Mn at former position of interface after first isothermal holding at T_1 and redistribution of interstitial alloying element around the interface. In type H-I, the profiles show a spike of Mn at the interface, the broadened bulge of Mn at former position of interface formed after first isothermal holding at T_1 and redistribution of interstitial alloying element around the interface. In type I, the profiles simply contain a spike of Mn at the interface and redistribution of interstitial alloying element around the interface. Finally, in type I-H, in addition to the spike of Mn at the interface and the zig-zag partitioning of Mn at the former position of the interface after the second isothermal holding at T_2, the profiles show redistribution of the interstitial alloying element around the interface.

The non-equilibrium transformation stage during heating in type I experiment is attributed to the incomplete redistribution of interstitial elements around the interface before subsequent variation of the temperature. In the Fe-0.1C-0.5Mn and Fe-0.5Mn systems, as a result of the relatively fast diffusion of carbon in austenite [32] and low carbon content, the length of the non-equilibrium transformation stage is very short. In the Fe-0.3N-0.5Mn alloy, the length of the non-equilibrium transformation stage is longer due to the slower diffusion of nitrogen in austenite [33] and associated decrease in the extent of nitrogen redistributed in type I cyclic route.

The stagnant stage during cyclic transformation is attributed to the spike of Mn at the interface as described by the local equilibrium partitioning model. The more partitioning of Mn at the interface, longer the stagnant stage is. Isothermal holding during cyclic transformation promotes partitioning of Mn at the interface and builds up a higher spike. This explains why the stagnant stage in the type I experiments is slightly shorter than that in type H experiments. In case of Fe-0.3N-0.5Mn alloy, the spike of Mn formed at the interface at the end of isothermal holding at T_1 in type H and type H-I is strong enough to hold the interface pinned until the end of cooling part. Thus no ferrite growth is observed after first isothermal holding in Figs. 2f and 4f.

The difference between the length of the stagnant stage in Fe-C-Mn, Fe-Mn and Fe-N-Mn alloys under CPPT experiments appears to support that Mn partitioning around the austenite/ferrite interface is affected by the presence of interstitial elements. According to the LE model, partitioning of Mn at the interface is controlled by equilibrium tie-lines. In order to better compare the partitioning behavior of C/N and Mn at the austenite/ferrite interface, it is valuable to study the evolution of interfacial concentrations of the solutes during cyclic transformation. Fig. 6a shows the interfacial concentration of C and Mn on the austenitic side of interface during type H cyclic experiment in Fe-0.1C-0.5Mn alloy projected on the isothermal sections of the Fe-C-Mn phase diagram at three critical temperatures. The time, temperature and interface position corresponding to each combination of interfacial C and Mn concentrations are shown in Fig. 6b and c. The migration of the interface during the isothermal direct transformation stages at $T_1 = 1048K(775\,^{\circ}C)$ and $T_2 = 1098K(825\,^{\circ}C)$, shown by C_1 to C_2 and C_4 to C_5, are accompanied by slight changes in the interfacial concentrations of both C and Mn along the austenitic boundary of the phase diagram at T_1 and T_2. The stagnant stages shown by C_2 to C_3 and C_5 to C_6, correspond to substantial changes of the Mn concentration at the interface. During the non-isothermal direct transformation stages of C_3 to C_4 and C_6 to C_7, the Mn concentrations are almost unchanged and the interface migration is accompanied by a considerable change in the interfacial concentration of C. The information in Fig. 6a suggests that in the Fe-C-Mn alloy the stagnant stage proceeds under to the partitioning local equilibrium (PLE) condition and transformation stages proceed under the negligible-partitioning local equilibrium (NPLE) condition.

The projected interfacial concentrations of N and Mn for type H CPPT experiment in Fe-0.3N-0.5Mn and corresponding time, temperatures and interface positions are shown in Fig. 6 d–f. Similar to Fe-C-Mn system, the kinetics of the transformation stage (N_1 to N_2) and stagnant stages (N_2 to N_3, N_3 to N_4 and N_4 to N_5) in the Fe-N-Mn system are explainable by transitions between interface migration under PLE and NPLE thermodynamic conditions. In this system, unlike the Fe-C-Mn system, the transitions in the interfacial concentration of elements on the austenitic side of interface during heating from T_1 to T_2 and cooling from T_2 to T_1 occurs only in one step of substantial variations in concentrations of both N and Mn, which corresponds to the PLE thermodynamic condition. As it can be seen in the isothermal sections of the phase diagrams in Fig. 6, thermodynamic equilibrium between the austenite and ferrite phases in the Fe-N-Mn system forms with higher interfacial concentrations of N and Mn than C and Mn in Fe-C-Mn. In other words, nitrogen stimulates partitioning of Mn and the build-up of an interfacial spike, more than C during the isothermal austenite to ferrite phase transformation at T_1. This implies that more Mn partitioning is required for the back migration of the interface, as well as the N partitioning to satisfy the LE condition at the interface. For the applied heating rate which is the same in both Fe-C-Mn and Fe-N-Mn systems, before the N has diffused enough to make the interface move under NPLE condition, the sample temperature has already reached the inversion temperature T_2 and a new equilibrium with lower interfacial Mn concentration was established at the interface which requires even more partitioning of Mn. The PLE thermodynamic condition observed in the cooling part from T_2 to T_1 can also be explained in such a way. This suggests that the thermodynamic transitions from NPLE to PLE in Fe-N-Mn system similar to those in Fe-C-Mn are expected to occur if very low heating and cooling rates are applied during the cyclic experiment.

The inverse transformation stage during CPPT experiments shows up if the partitioning of the interstitial elements around the interface does not disappear prior to the rapid alternation of temperature regime and the interface continues its migration in a wrong direction. In order to better understand the differences in solute partitioning in the F-C-Mn, Fe-Mn and F-N-Mn systems at different temperatures it is useful to examine at the equilibrium partitioning coefficients shown in Fig. 7. These coefficients were defined as $X^{\gamma}_{equilibrium}/X^{\alpha}_{equilibrium}$, where X is mole fraction of each

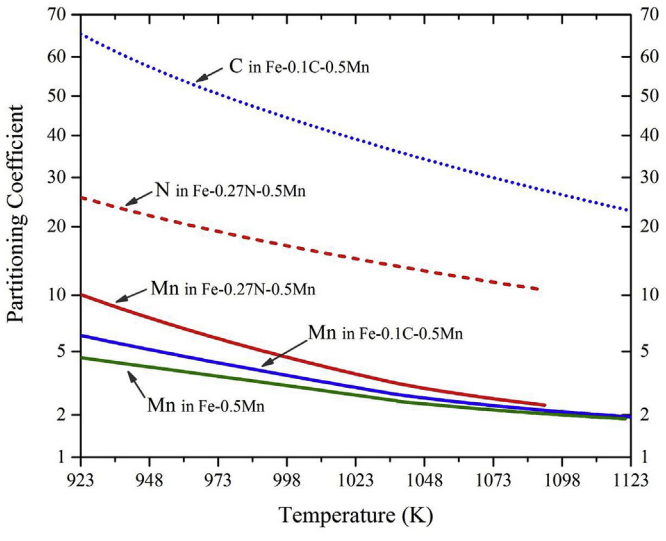

Fig. 7. Partitioning coefficient of C, N and Mn in different systems.

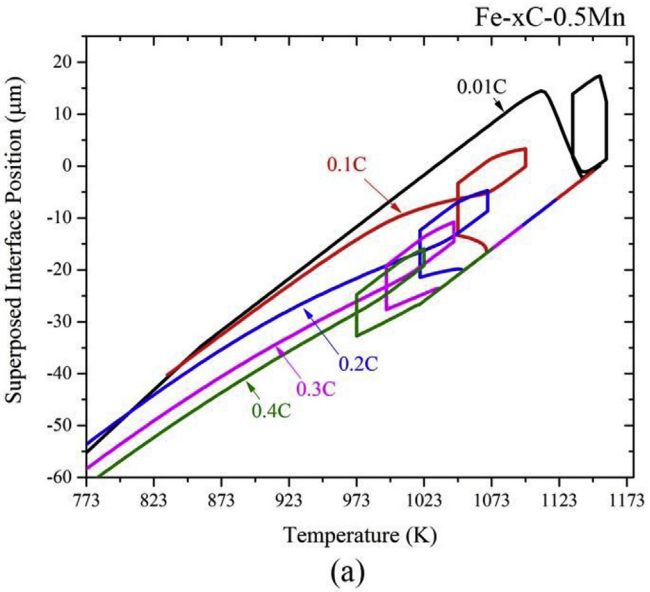

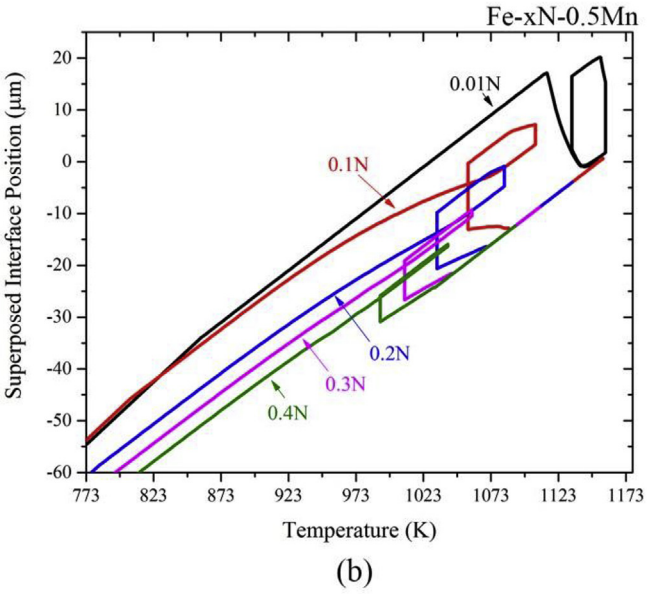

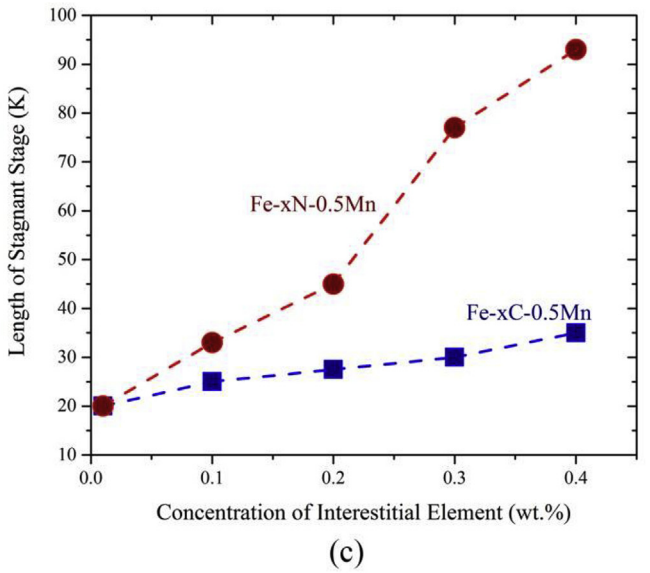

alloying element. The partitioning coefficient of Mn is higher in the Fe-N-Mn system than it is in the Fe-C-Mn system. As a result, ferrite formation under equilibrium conditions in the Fe-N-Mn system requires more partitioning of Mn than ferrite formation in Fe-C-Mn at similar temperatures. Nitrogen partitions less than carbon during austenite decomposition, however, its lower diffusivity promotes the longer inverse transformation stages observed in type I cyclic experiments. Mn in the Fe-Mn binary system has the lowest partitioning coefficient suggesting that Mn tends to partition even in an interstitial-free system, but its partitioning is promoted in the presence of interstitial elements. The stagnant stage of 20K in Fe-0.5Mn alloy indirectly endorses that Mn interaction with the migrating interface in interstitial-free binary system should be substantial. This suggests, in contrast to other reports [13,34–36], that the kinetics of austenite to ferrite transformation in Fe-X systems alloyed with substitutional elements is a mixed-mode and controlled also by diffusion [37]. The analysis of partitioning coefficient of alloying elements in above indicates that experimental observations in this study for the base composition used with 0.5 mass% Mn are well explainable just with considering effect of C and N on the equilibrium thermodynamic partitioning of Mn between ferrite and austenite phases. However, we should emphasize that this does not mean that for other Mn contents, or in multi-component alloys (such as Fe-C-Mn-Si), or slower interface velocities (such as during decarburization reactions), an interaction between the C/Mn at the interface is not important to take into account.

In our study, CPPT experiments provide indirect evidence for noticeable Mn partitioning at the austenite/ferrite interface in Fe-C/N-Mn systems. The difference between stagnant stages in type H cyclic experiments can only be explained by different partitioning behavior of Mn in the presence and absence of different interstitial elements. However, a counter argument opposing this can arise from selection of different critical temperatures for CPPT experiments in different systems. In order to remove the effect of temperature, further investigation on the effect of C and N and their absence on the length of stagnant stage at different temperatures is performed through systematic simulation of type H CPPT experiment using the LE model in Fe-xC-0.5Mn (Fig. 8a) and Fe-xN-0.5Mn (Fig. 8b) systems (x = 0.01 to 0.4 wt%). As it can be seen in Fig. 8c, the stagnant stage, or as explained above spike of Mn, appears also in the interstitial-free system of Fe-0.5Mn and higher concentration of interstitial elements leads to a longer stagnant stage. In addition, nitrogen clearly creates a longer stagnant stage than the equivalent C containing system. As a final point, it is worth noting that the length of the stagnant stage predicted by LE model in Fig. 8c is quite comparable with the experimentally measured values in Figs. 2–4. This suggests that the concentration of interstitial elements can be estimated indirectly by measuring the length of stagnant stage.

7. Conclusions

In our study, cyclic partial phase transformation experiments have been successfully used to study the effect of interstitial elements (carbon and nitrogen) and their absence on the partitioning behavior of Mn in a Fe-0.5Mn steel. The results of experiments and local equilibrium modelling are comparable and confirm.

1 Indirect evidence of Mn partitioning at austenite/ferrite interface in absence of interstitial elements

Fig. 8. Results of systematic type H CPPT simulations in a) Fe-C-Mn and b) Fe-N-Mn system, c) length of stagnant stage during type H CPPT in Fe-C-Mn and Fe-N-Mn systems.

2 Nitrogen promotes Mn partitioning at interface more than carbon
3. Local equilibrium model can semi-quantitatively capture the experimental observations in cyclic experiments

Acknowledgment

This research was funded by ArcelorMittal, France. H. Farahani and S. van der Zwaag acknowledge Dr. Didier Huin from ArcelorMittal for continuous support.

References

[1] M. Gouné, F. Danoix, J. Ågren, Y. Bréchet, C.R. Hutchinson, M. Militzer, G. Purdy, S. van der Zwaag, H. Zurob, Overview of the current issues in austenite to ferrite transformation and the role of migrating interfaces therein for low alloyed steels, Mater. Sci. Eng. R Rep. 92 (2015) 1–38, https://doi.org/10.1016/j.mser.2015.03.001.
[2] D.E. Coates, Diffusion controlled precipitate growth in ternary systems: II, Metall. Trans. 4 (1973) 1077–1086, https://doi.org/10.1007/BF02645611.
[3] D.E. Coates, Diffusion-controlled precipitate growth in ternary systems I, Metall. Trans. 3 (1972) 1203–1212, https://doi.org/10.1007/BF02642453.
[4] M. Hillert, J. Ågren, On the definitions of paraequilibrium and orthoequilibrium, Scripta Mater. 50 (2004) 697–699, https://doi.org/10.1016/j.scriptamat.2003.11.020.
[5] M. Hillert, J. Odqvist, J. Ågren, Interface conditions during diffusion-controlled phase transformations, Scripta Mater. 50 (2004) 547–550, https://doi.org/10.1016/j.scriptamat.2003.10.027.
[6] H.S. Zurob, C.R. Hutchinson, Y. Bréchet, H. Seyedrezai, G.R. Purdy, Kinetic transitions during non-partitioned ferrite growth in Fe–C–X alloys, Acta Mater. 57 (2009) 2781–2792, https://doi.org/10.1016/j.actamat.2009.02.029.
[7] H.S. Zurob, C.R. Hutchinson, A. Béché, G.R. Purdy, Y.J.M. Bréchet, A transition from local equilibrium to paraequilibrium kinetics for ferrite growth in Fe–C–Mn: a possible role of interfacial segregation, Acta Mater. 56 (2008) 2203–2211, https://doi.org/10.1016/j.actamat.2008.01.016.
[8] M. Enomoto, Influence of solute drag on the growth of proeutectoid ferrite in Fe–C–Mn alloy, Acta Mater. 47 (1999) 3533–3540, https://doi.org/10.1016/S1359-6454(99)00232-3.
[9] V.G. Gavriljuk, J. Rawers, B.D. Shanina, H. Berns, Nitrogen and carbon in austenitic and martensitic steels: atomic interactions and structural stability, Mater. Sci. Forum 426–432 (2003) 943–950 doi:10.4028/www.scientific.net/MSF.426-432.943.
[10] V.G. Gavriljuk, Austenite and martensite in nitrogen-, carbon- and hydrogen-containing iron alloys: similarities and differences, Mater. Sci. Eng., A 438 (2006) 75–79, https://doi.org/10.1016/j.msea.2006.01.097.
[11] Y. Liu, F. Sommer, E.J. Mittemeijer, Abnormal austenite-ferrite transformation kinetics of ultra-low-nitrogen Fe-N alloy, Metall. Mater. Trans. 39 (2008) 2306–2318, https://doi.org/10.1007/s11661-008-9601-7.
[12] N.K. Balliger, R.W.K. Honeycombe, The effect of nitrogen on precipitation and transformation kinetics in vanadium steels, Metall. Trans. A 11 (1980), https://doi.org/10.1007/BF02654566.
[13] A.T.W. Kempen, F. Sommer, E.J. Mittemeijer, The kinetics of the austenite–ferrite phase transformation of Fe-Mn: differential thermal analysis during cooling, Acta Mater. 50 (2002) 3545–3555, https://doi.org/10.1016/S1359-6454(02)00149-0.
[14] M. Guo, D. Panahi, H. Van Landeghem, C.R. Hutchinson, G. Purdy, H.S. Zurob, A comparison of ferrite growth kinetics under denitriding and decarburizing conditions, Metall. Mater. Trans. 46 (2015) 2449–2454, https://doi.org/10.1007/s11661-015-2851-2.
[15] H.P. Van Landeghem, B. Langelier, D. Panahi, G.R. Purdy, C.R. Hutchinson, G.A. Botton, H.S. Zurob, Solute segregation during ferrite growth: solute/interphase and substitutional/interstitial interactions, JOM (J. Occup. Med.) 68 (2016) 1329–1334, https://doi.org/10.1007/s11837-016-1852-y.
[16] Y. Yogo, K. Tanaka, H. Ikehata, N. Iwata, K. Nakanishi, T. Ishikawa, Calculation for grain growth rate of carbon steels by solute drag model considering segregation effect of each substitutional element, Mater. Sci. Technol. 27 (2011) 1593–1698, https://doi.org/10.1179/1743284710Y.0000000016.
[17] G. Purdy, J. Ågren, A. Borgenstam, Y. Bréchet, M. Enomoto, T. Furuhara, E. Gamsjager, M. Gouné, M. Hillert, C. Hutchinson, M. Militzer, H. Zurob, ALEMI: a ten-year history of discussions of alloying-element interactions with migrating interfaces, Metall. Mater. Trans. 42 (2011) 3703–3718, https://doi.org/10.1007/s11661-011-0766-0.
[18] Z. Dai, X. Wang, J. He, Z. Yang, C. Zhang, H. Chen, Effect of interfacial Mn partitioning on carbon partitioning and interface migration during the quenching and partitioning process, Metall. Mater. Trans. 48 (2017) 3168–3174, https://doi.org/10.1007/s11661-017-4121-y.
[19] H. Chen, S. van der Zwaag, The effect of interfacial element partitioning on ferrite and bainite formation, JOM (J. Occup. Med.) 68 (2016) 1320–1328, https://doi.org/10.1007/s11837-016-1848-7.
[20] M. Hillert, Nature of local equilibrium at the interface in the growth of ferrite from alloyed austenite, Scripta Mater. 46 (2002) 447–453, https://doi.org/10.1016/S1359-6462(01)01257-X.
[21] A.T. Wicaksono, M. Militzer, Interaction of C and Mn in a $\sum$3 grain boundary of bcc iron, IOP Conf. Ser. Mater. Sci. Eng. 219 (2017) 012044, https://doi.org/10.1088/1757-899X/219/1/012044.
[22] W.W. Sun, H.S. Zurob, C.R. Hutchinson, Coupled solute drag and transformation stasis during ferrite formation in Fe-C-Mn-Mo, Acta Mater. 139 (2017) 62–74, https://doi.org/10.1016/J.ACTAMAT.2017.08.010.
[23] C. Qiu, H.S. Zurob, C.R. Hutchinson, The coupled solute drag effect during ferrite growth in Fe–C–Mn–Si alloys using controlled decarburization, Acta Mater. 100 (2015) 333–343. http://www.sciencedirect.com/science/article/pii/S1359645415006527. (Accessed 25 September 2017).
[24] M. Enomoto, H.I. Aaronson, Nucleation kinetics of proeutectoid ferrite at austenite grain boundaries in Fe-C-X alloys, Metall. Trans. A 17 (1986) 1385–1397, https://doi.org/10.1007/BF02650120.
[25] S.E. Offerman, N.H. van Dijk, J. Sietsma, S. Grigull, E.M. Lauridsen, L. Margulies, H.F. Poulsen, M.T. Rekveldt, S. van der Zwaag, Grain nucleation and growth during phase transformations, Science 298 (2002) 1003–1005, https://doi.org/10.1126/science.1076681.
[26] H. Chen, S. van der Zwaag, An overview of the cyclic partial austenite-ferrite transformation concept and its potential, Metall. Mater. Trans. (2016) 1–10, https://doi.org/10.1007/s11661-016-3826-7.
[27] H. Chen, B. Appolaire, S. van der Zwaag, Application of cyclic partial phase transformations for identifying kinetic transitions during solid-state phase transformations: experiments and modeling, Acta Mater. 59 (2011) 6751–6760, https://doi.org/10.1016/j.actamat.2011.07.033.
[28] H. Chen, S. van der Zwaag, Analysis of ferrite growth retardation induced by local Mn enrichment in austenite created by prior interface passages, Acta Mater. 61 (2013) 1338–1349, https://doi.org/10.1016/j.actamat.2012.11.011.
[29] H. Chen, Cyclic Partial Phase Transformations in Low Alloyed Steels: Modeling and Experiments, Delft University of Technology, 2013, 10.4233/UUID:66975E4A-4B2D-4933–4995C5-F180B6605882.
[30] A.G. Svyazhin, J. Siwka, Z. Skuza, A. Hutny, Gas blow-holes forming in nitrogen iron alloys and steels during their crystallization, in: Mater. Sci. Forum, 1999.
[31] J.-O. Andersson, T. Helander, L. Höglund, P. Shi, B. Sundman, Thermo-Calc & DICTRA, computational tools for materials science, Calphad 26 (2002) 273–312, https://doi.org/10.1016/S0364-5916(02)00037-8.
[32] K. Nakajima, M. Apel, I. Steinbach, The role of carbon diffusion in ferrite on the kinetics of cooperative growth of pearlite: a multi-phase field study, Acta Mater. 54 (2006) 3665–3672, https://doi.org/10.1016/j.actamat.2006.03.050.
[33] S. Mändl, F. Scholze, H. Neumann, B. Rauschenbach, Nitrogen diffusivity in expanded austenite, Surf. Coating. Technol. 174–175 (2003) 1191–1195, https://doi.org/10.1016/S0257-8972(03)00454-7.
[34] J. Hamada, M. Enomoto, T. Fujishiro, T. Akatsuka, In-situ observation of the growth of massive ferrite in very low-carbon Fe-Mn and Ni alloys, Metall. Mater. Trans. 45 (2014) 3781–3789, https://doi.org/10.1007/s11661-014-2336-8.
[35] J.J. Wits, T.A. Kop, Y. van Leeuwen, J. Seitsma, S. van der Zwaag, A study on the austenite-to-ferrite phase transformation in binary substitutional iron alloys, Mater. Sci. Eng., A 283 (2000) 234–241, https://doi.org/10.1016/S0921-5093(00)00735-8.
[36] G.P. Krielaart, S. van der Zwaag, Kinetics of $\gamma \rightarrow \alpha$ phase transformation in Fe-Mn alloys containing low manganese, Mater. Sci. Technol. 14 (1998) 10–18, https://doi.org/10.1179/mst.1998.14.1.10.
[37] M. Enomoto, X.L. Wan, In situ observation of austenite growth during continuous heating in very-low-carbon Fe-Mn and Ni alloys, Metall. Mater. Trans. 48 (2017) 1572–1580, https://doi.org/10.1007/s11661-017-3961-9.